frontiers | Frontiers in Materials

TYPE Original Research
PUBLISHED 17 June 2024
DOI 10.3389/fmats.2024.1425653



OPEN ACCESS

EDITED BY
Junfei Zhang,
Hebei University of Technology, China

REVIEWED BY
Dominic E. L. Ong,
Griffith University, Australia
Jue Li,
Chongqing Jiaotong University, China

*CORRESPONDENCE
Xinxing Xu,
2019054@dgpt.edu.cn

RECEIVED 30 April 2024
ACCEPTED 28 May 2024
PUBLISHED 17 June 2024

CITATION
Xu X and Yan X (2024), Experiment on MICP-solidified calcareous sand with different rubber particle contents and sizes.
*Front. Mater.* 11:1425653.
doi: 10.3389/fmats.2024.1425653



# Experiment on MICP-solidified calcareous sand with different rubber particle contents and sizes

Xinxing Xu* and Xinning Yan

School of Architecture, Dongguan Polytechnic, Dongguan, China

Microbially induced calcite precipitation (MICP) is a new environmentally friendly technology, with the ability to improve the mechanical properties of calcareous sand. Rubber is a high-compressibility material with a higher damping ratio than that of calcareous sand. In this study, calcareous sand was replaced by equal volume contents (0%, 1%, 3%, 5%, 7%, and 9%) and different sizes (0–1, 1–2, and 2–3 mm) of rubber, and a series of water absorption and unconfined compressive strength (UCS) tests were conducted on MICP-solidified rubber–calcareous sand (MRS). The results showed that the water absorption is reduced when the rubber content is larger. The UCS of 0–1-mm MRS decreased with the increase in rubber content. For 1–2-mm and 2–3-mm MRS, the UCS was improved by 11.30% and 15.69%, respectively, compared with the clean sand. Adding rubber promoted the formation of calcium carbonate, but the strength and stiffness of rubber particles were lower than those of the calcareous sand. Therefore, higher rubber content weakened the sand frame bearing system, and the UCS decreased when the rubber content was more than 5%. Moreover, a large amount of 0–1-mm rubber led to the increase in transverse deformation of the samples, which caused the acceleration of the destruction of the sand structure. The water absorption of 0–1-mm MRS was higher than that of 1–2-mm and 2–3-mm MRS, but the UCS of 0–1-mm MRS was lower. The best rubber size is 1–2 mm and 2–3 mm, and the best rubber content is 3%–5%. The outcome of this study may, in the authors' view, prove beneficial in improving the strength of calcareous sand when it is reinforced by MICP-combined rubber.

KEYWORDS

**microbially induced calcite precipitation, rubber, content, size, water absorption, unconfined compressive strength**

## 1 Introduction

Calcareous sand is a kind of special marine sediment formed by the complex physical, chemical, and biological processes of coral reef debris, algae, shells, and other debris in the marine environment. Since calcareous sand is formed mainly from coral reefs through long-term geological processes, it retains the characteristics of multi-porosity and complex particle shapes inside the coral reef skeleton (Shahnazari and Rezvani, 2013; Bai et al., 2023). Compared with quartz sand, calcareous sand has a more irregular shape, is porous and brittle, and has lower strength. The calcareous sand must be reinforced if it is to be used as a foundation material for engineering construction

(Wang et al., 2020; Bai et al., 2021). As a new foundation reinforcement method, microbially induced calcite precipitation (MICP) technology has a potential application value in the fields of liquefiable sand layers (Riveros and Sadrekarimi, 2020), roadbeds (Xiao et al., 2022), and foundation pit slope reinforcement (Cheng et al., 2021). Compared with the traditional cement reinforcement method, the MICP treatment method is environmentally friendly, has low energy consumption, and is sustainable (Wang et al., 2017; Castro-Alonso et al., 2019; Su et al., 2022). In island construction, compared to traditional cement solidification, MICP has two major advantages: the first is the abundant $Cl^-$ and $SO_4^{2-}$ in the marine environment that will cause corrosion to ferroconcrete but have little impact on MICP treatment (Saleem et al., 1996); the second is the slightly alkaline environment of the ocean that is conducive to the reaction of microorganisms (Stocks-Fischer et al., 1999). Therefore, MICP is more suitable for applications in island construction.

Due to the perfect control effect and advantages of MICP technology, numerous scholars have studied MICP-solidified sand in recent years. The research showed that MICP reinforcement can improve strength (DeJong et al., 2006; Montoya and DeJong, 2015; Aamir et al., 2018), stiffness (van Paassen et al., 2010; O'Donnell and Kavazanjian, 2015), and liquefaction resistance (Montoya et al., 2013; Xiao et al., 2018; Shan et al., 2022a; Zhao et al., 2022) and reduce permeability (Chu et al., 2013; Cuthbert et al., 2013; Phillips et al., 2016) and deformation (Yuan et al., 2022) of soil. In practical engineering construction, MICP technology is also constantly applied, such as inhibition of dust (Fan et al., 2020), biopolymer improvement (Lee et al., 2019), and concrete self-repair (Nosouhian et al., 2016). In addition, some studies showed that the strength and ductility of sand can be improved by adding some additional materials, such as fiber and activated carbon (Harkes et al., 2010; Xiao et al., 2019; Zhao et al., 2020; Shan et al., 2022b).

However, few studies of MICP-solidified sand considered rubber particles as additives for MICP technology. Rubber itself is a high-compressibility material with Poisson's ratio of approximately 0.5, which is higher than that of calcareous sand (Wang et al., 2011; Hassanli et al., 2020). The damping ratio of rubber is relatively large, and adding rubber to the sand can improve its seismic performance (Anastasiadis et al., 2012). For the MICP-solidified rubber sand, Cui et al. (2021) found that the rubber particles contribute to improving the brittle behavior and reducing the dilation of MICP-solidified calcareous sand. Li (2021) showed that the rubber sand after MICP treatment is a good shock-damping material. The above study only selected a single rubber content and particle size, but the mechanical properties of calcareous sand after MICP treatment are affected by different contents and sizes of rubber particles.

Therefore, this study selected rubber particles of different sizes (0–1 mm, 1–2 mm, and 1–3 mm) from waste tires and added them to calcareous sand by volume ratio (0%, 1%, 3%, 5%, 7%, and 9%). Several groups of rubber–calcareous sand (RS) samples with different rubber contents and particle sizes were selected. A series of water absorption and unconfined compressive strength tests were carried out to investigate the effects of rubber content and size on the MICP-solidified RS. The investigation showed that adding 3%–5% rubber particles of 1–2 mm and 2–3 mm to calcareous sand could improve its strength. These findings provide a reliable experimental basis for rubber applications in calcareous sand foundation engineering.

TABLE 1 Physical and mechanical parameters of calcareous sand.

| Parameter | Value |
|---|---|
| $C_c$ | 1.170 |
| $C_u$ | 2.231 |
| $G_s$ | 2.76 |
| $D_{10}$ | 0.26 |
| $D_{30}$ | 0.42 |
| $D_{50}$ | 0.54 |
| $D_{60}$ | 0.58 |
| $e_{max}$ | 1.24 |
| $e_{min}$ | 0.80 |

## 2 Materials and test methods

### 2.1 Materials

The calcareous sand used in this study was obtained from Yongxing Island located in the South China Sea. The sand was cleaned with distilled water and dried in an oven at 60°C (the particle surface of calcareous sand would have become bark if overdried at or above 100°C) to remove large particle impurities in the original sand (Xiao et al., 2018). The physical and mechanical parameters are shown in Table 1. The grain size distribution of calcareous sand is shown in Figure 1. The grain size of the sand ranged from 0.2 to 1 mm, which was classed as poorly graded sand (SP) based on the Unified Soil Classification System (ASTM, 2017).

The rubber used in the experiments was taken from old waste tires, as shown in Figure 2. The old waste tires were cut into particles, and the steel wire was removed. After processing, the rubber particle-size control is less than 3 mm. After the screening, the rubber particle size ranged between 0.5 and 3 mm, average particle size $D_{50}$ is 1.5 mm, and bulk density is 0.51 g/cm$^3$. The rubbers are classified as rubber particles according to the Standard Practice for Use of Scrap Tires in Civil Engineering Applications (ASTM, 2020).

The strain *Sporosarcina pasteurii* was purchased from Guangdong Microbiological Conservation Center (GDMCC), China. The bacterial culture medium consisting of 20 g/L yeast extract, 10 g/L $(NH_4)_2SO_4$, and 1.6 g/L NaOH was first sterilized in a pressure steam sterilizer at 120°C for 20 min. Then, the bacteria were inoculated into the medium and cultured in a conical flask at 180 rpm and 28°C for 20 h. The concentration of the bacterial solution was detected using a spectrophotometer at a wavelength of 600 nm ($OD_{600}$) (Zhao et al., 2020). The $OD_{600}$ of the bacterial solution reached 1.0–1.8 ($10^7$ cells/mL). The urease activity of the final bacterial solution was approximately 4.75 mM urea/min, which

TABLE 2 Rubber volume and mass table.

| Ratio $V_r/V_s$ (%) | $V_s$ ($cm^3$) | $V_r$ ($cm^3$) | $V_t$ ($cm^3$) | $m_s$ (g) | $m_r$ (g) |
|---|---|---|---|---|---|
| 0 | 47.525 | 0 | 47.525 | 131.17 | 0 |
| 1 | 47.054 | 0.471 | 47.525 | 129.87 | 0.24 |
| 3 | 46.141 | 1.384 | 47.525 | 127.35 | 0.71 |
| 5 | 45.262 | 2.263 | 47.525 | 124.92 | 1.15 |
| 7 | 44.416 | 3.109 | 47.525 | 122.59 | 1.59 |
| 9 | 43.601 | 3.924 | 47.525 | 120.34 | 2.00 |

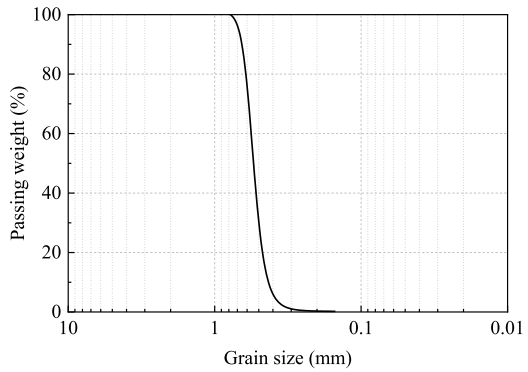


FIGURE 1
Grain size distribution of the calcareous sand.

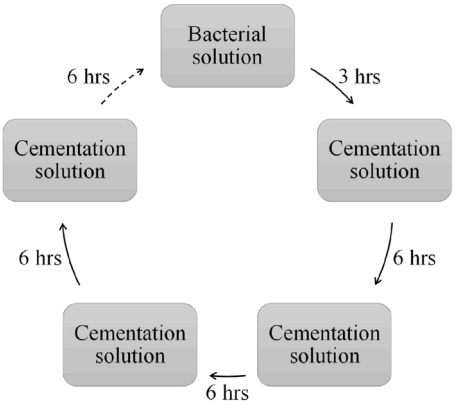


FIGURE 3
One round of grouting.

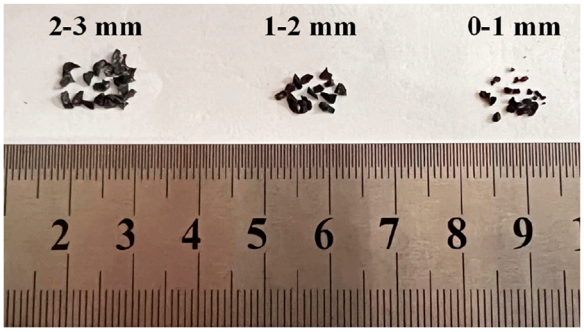


FIGURE 2
Rubber particles.

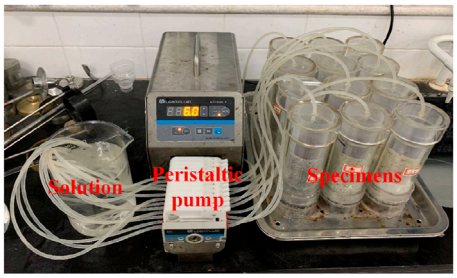


FIGURE 4
Grouting procedure of the peristaltic pump.

was measured using a conductivity meter (Whiffin et al., 2007). Then, 55.5 g calcium chloride and 30 g $CO(NH_2)_2$ were weighed first, and the reagents were added to 1 L distilled water. Finally, the cementation solution of 0.5 mol/L $CaCl_2$ and urea was obtained.

## 2.2 Test methods

The cylinder specimens with 39.1-mm diameter and 80-mm height were used in this study. The relative density of the sample was controlled at 50% (i.e., 131.17 g sand). The rubber particle size was chosen as 0–1 mm, 1–2 mm, and 2–3 mm. The rubber and calcareous sand were mixed to form RS in proportion to volume (i.e., the volume of sand $V_s$ over the volume of rubber $V_r$ was equaled to 0%, 1%, 3%, 5%, 7%, and 9%). The total volume $V_t$ of the solid materials was constant (i.e., volume of sand $V_s$ plus the volume of rubber $V_r$). The volume of sand $V_s$ and the volume of rubber $V_r$ could be calculated. Finally, the mass of the rubber $m_r$ and $m_s$ could be calculated, as shown in Table 2. The void ratio $e$ of each sample prepared in this way was consistent, which could ensure the

TABLE 3 Results of rubber–sand with different particle sizes and contents.

| No. | Rubber particle (mm) | Rubber content (%) | $CaCO_3$ $W_{Ca}$ (%) | Water absorption $\omega$ (%) | UCS (MPa) |
|---|---|---|---|---|---|
| $U_0$ | / | 0 | 20.28 | 21.61 | 2.394 |
| $U_{01\text{-}1}$ | 0–1 | 1 | 19.29 | 19.48 | 2.032 |
| $U_{01\text{-}3}$ | | 3 | 19.60 | 17.96 | 1.870 |
| $U_{01\text{-}5}$ | | 5 | 19.74 | 17.85 | 1.058 |
| $U_{01\text{-}7}$ | | 7 | 20.12 | 19.48 | 0.675 |
| $U_{01\text{-}9}$ | | 9 | 20.75 | 19.04 | 0.350 |
| $U_{12\text{-}1}$ | 1–2 | 1 | 22.43 | 21.55 | 2.350 |
| $U_{12\text{-}3}$ | | 3 | 22.64 | 21.34 | 2.664 |
| $U_{12\text{-}5}$ | | 5 | 23.55 | 18.07 | 2.458 |
| $U_{12\text{-}7}$ | | 7 | 24.16 | 17.29 | 1.801 |
| $U_{12\text{-}9}$ | | 9 | 24.63 | 14.89 | 1.307 |
| $U_{23\text{-}1}$ | 2–3 | 1 | 21.76 | 21.28 | 2.300 |
| $U_{23\text{-}3}$ | | 3 | 22.26 | 20.02 | 2.574 |
| $U_{23\text{-}5}$ | | 5 | 22.64 | 19.53 | 2.769 |
| $U_{23\text{-}7}$ | | 7 | 23.26 | 19.16 | 1.982 |
| $U_{23\text{-}9}$ | | 9 | 23.60 | 16.77 | 1.484 |

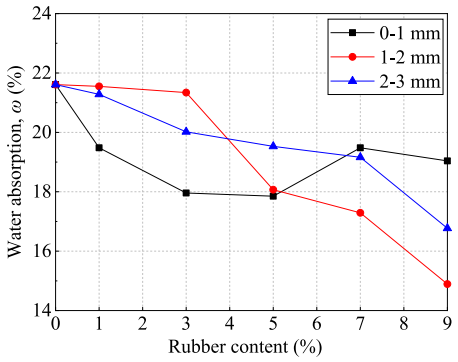


FIGURE 5
Results of water absorption tests.

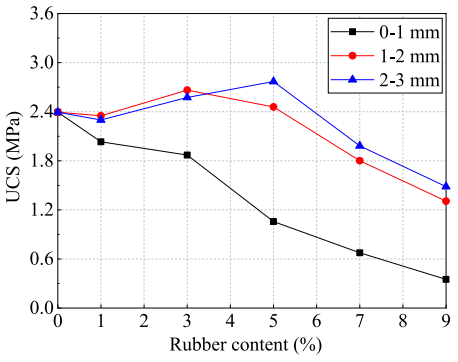


FIGURE 6
Results of UCS tests.

comparability between each sample. The RS was compacted into the PVC mold in four layers. Each layer was slightly compacted using a compaction tool.

A peristaltic pump was used for cyclic grouting. The solution was injected from the top of the sample and flowed to the bottom (Omoregie et al., 2023). The grouting rate was controlled at 1.0 mL/min. The rate of injection has little effect on the "internal erosion" of the sand grains (Liu et al., 2017; Omoregie et al., 2024). The bacterial solution was injected and stood for 3 h, and then the cementation solution was injected every 6 h four times, where each injection volume was one specimen pore volume. The above grouting process is one round, as shown in Figure 3. A total of six

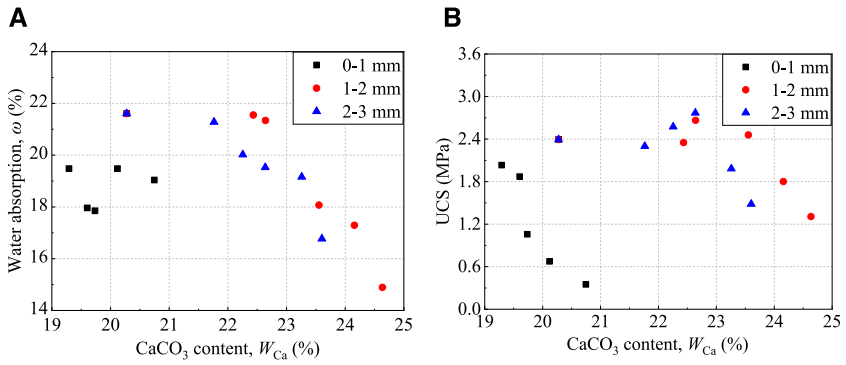


FIGURE 7
Relationship between $W_{Ca}$ and **(A)** $\omega$ and **(B)** UCS.

rounds of grouting were carried out. A photograph of the grouting is shown in Figure 4. The samples were weighed before grouting, and the mass was $m_b$. The MICP-solidified samples were dried in an oven at 60°C for 48 h. Then, the samples were taken out and weighed, and the mass was recorded as $m_a$. The calcium carbonate content ($W_{Ca}$) is as follows Eq. 1.

$$W_{Ca} = \frac{m_a - m_b}{m_b} \times 100\% \quad (1)$$

The water absorption can be used to indirectly analyze and evaluate the development degree of the open pores and internal cracks in the samples. The steps of the test were as follows: the MICP-solidified RS (MRS) was dried in an oven at 60°C for 48 h, and its mass is called $m_a$. The samples were then placed in a tank with distilled water and left to stand for 24 h. Then, the samples were taken out, and the surface residual water was quickly removed, with its mass recorded as $m_w$. The water absorption $\omega$ was calculated according to Eq. 2 (Zhao et al., 2021):

$$\omega = \frac{m_w - m_a}{m_a} \times 100\% \quad (2)$$

A series of unconfined compressive strength (UCS) tests were performed to measure the strength of the MRS. The specimens used in the UCS test were dried in an oven at 60°C for 48 h. A YAW-S300 automatic liquid crystal pressure testing machine was used for the test. A loading rate of 1.0 mm/min was adopted. Table 3 lists the detailed test results of different rubber particles and contents.

# 3 Results

## 3.1 Results of the water absorption test

Figure 5 shows the curve of the relationship between water absorption $\omega$ and rubber content. As shown in Figure 5, $\omega$ of MRS in each rubber particle size was lower than that of $U_0$. For the 0–1-mm MRS, $\omega$ showed a significant change compared with $U_0$ and decreased by 9.86% when the rubber content was 1%. Within 1%–5% of rubber content, $\omega$ decreased with the increase in the rubber content. Within 5%–7%, $\omega$ increased with the increase in the rubber content, but the decrease was not obvious. When the rubber content was 5%, $\omega$ was 17.85%, which was 17.38% lower than that of $U_0$. For the 1–2-mm and 2–3-mm MRS, $\omega$ had little change when the rubber content was 1%. When the rubber content was 1%–9%, $\omega$ gradually decreased with the increase in the rubber content and reached a minimum when the rubber content was 9%, which was 14.89% and 16.77%, respectively. Compared with $U_0$, $\omega$ decreased by 31.09% and 22.40%. Moreover, when the rubber content was below 5%, $\omega$ of the 0–1-mm MRS was lower than that of the 1–2 mm and 2–3 mm MRS. When the rubber content was above 5%, $\omega$ of the 1–2-mm and 2–3-mm MRS continued to decrease, and $\omega$ of the 1–2-mm MRS was lower than that of the 0–1 mm and 2–3 mm MRS. It indicates that $\omega$ was reduced due to the large rubber content and particle size.

## 3.2 Results of the UCS test

Figure 6 shows the results of the UCS test of MICP-solidified sand with different rubber contents and particle sizes. As shown in Figure 6, for the 0–1-mm MRS, the UCS gradually decreased with the increase in the rubber content. For the 1–2-mm and 2–3-mm MRS, the UCS of MICP-solidified sand increased first and then decreased with the increase in the rubber content. The 1–2-mm MRS reached a peak value when the rubber content was 3%, and the UCS was 2.664 MPa, which had an 11.30% increase compared to $U_0$. The 2–3-mm MRS reached a peak value when the rubber content was 5%, and the peak value was 2.769 MPa, which was increased by 15.69% compared to $U_0$. In general, with the increase in the rubber content, the UCS of MICP-solidified sand decreased, but when the rubber particle size was 1–2 mm and 2–3 mm, the appropriate rubber content improved the UCS of MICP-solidified sand. When the rubber particle size increased from 0–1 mm to 1–2 mm, the UCS of all samples increased, and the fastest growth was observed in the group with 5% rubber content, where the UCS increased from 1.058 MPa to 2.458 MPa. When the rubber particle size increased to 2–3 mm, the UCS of the two groups with 1% and 3% rubber content decreased, while that of the other groups increased.

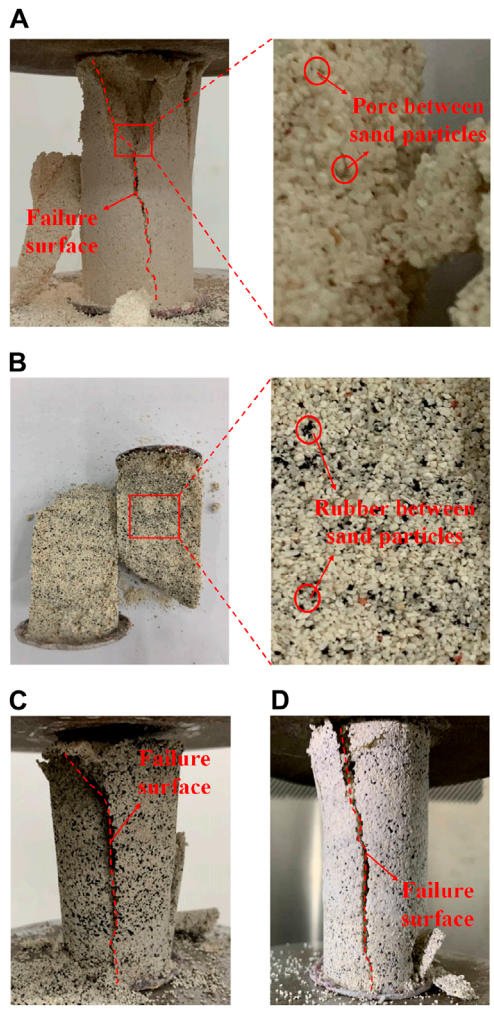


FIGURE 8
Samples after UCS tests. **(A)** $U_0$. **(B)** $U_{01\text{-}5}$. **(C)** $U_{12\text{-}7}$. **(D)** $U_{23\text{-}5}$.

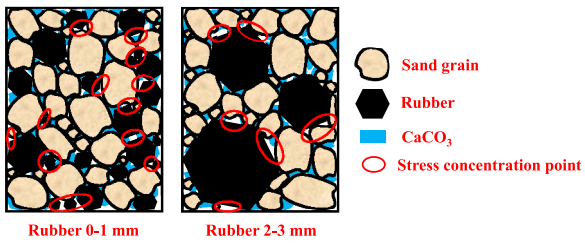


FIGURE 9
Diagram of the stress concentration effect.

## 3.3 Results of the $CaCO_3$ content

Figure 7 shows the relationship between the $CaCO_3$ content ($W_{Ca}$) and water absorption $\omega$ and UCS. As shown in Figure 7A, for the MICP-solidified sand with different particle sizes, $W_{Ca}$ increased with the increase in the rubber content, and $\omega$ decreased with the increase in $W_{Ca}$. However, as shown in Figure 7B, the UCS did not increase with the increase in $W_{Ca}$ as in previous studies (Aamir et al., 2018; Zhao et al., 2018; Ma et al., 2021). The specific mechanism analysis is described in the following section.

# 4 Mechanism analysis

## 4.1 Influence of the rubber content

Calcareous sand is a porous material, while rubber particle is a material with a rough surface and dense interior. Replacing calcareous sand with rubber particles in equal volume reduces the pore defects of MICP-solidified sand. In addition, the rubber particles being torn on the failure surface of MRS are fewer than that of $U_0$ (Figures 8A–D). The incorporation of rubber can promote the formation of calcium carbonate, and "calcareous sand–$CaCO_3$ crystal–rubber particle" bonding action makes the sample denser, which enhances the interface force between rubber particles and sand particles. The combined action of rubber and MICP treatment inhibits the generation and development of initial cracks in the MICP-solidified samples. Therefore, $\omega$ decreased and UCS increased with the increase in the rubber content.

However, the strength and stiffness of rubber particles are much lower than those of calcareous sand (Zhou et al., 2023). The equivalent volume replacement of rubber in calcareous sand directly weakened the strength and stiffness of the original pure calcareous sand frame bearing system. Moreover, the rubber particles are easy to aggregate in the process of mixing with calcareous sand. This phenomenon is more likely to occur when the rubber content is high. Therefore, although $\omega$ increased with the increase in the rubber content, the UCS decreased when the rubber content was more than 5%, as shown in Figure 5 and Figure 6.

## 4.2 Influence of rubber size

First, rubber is a kind of polymer organic matter, and calcareous sand is a kind of inorganic material (Gersten et al., 1999; Frutos et al., 2016). The physical form and chemical structure of these two materials have obvious differences. They can only produce physical operations without chemical reactions, which leads to a lack of connection between them. It is difficult to form a whole structure, so the rubber and calcareous sand mixture forms a weaker interface. During the loading, the failure of the internal structure of the MRS started from the weak interface between rubber and sand. The smaller the rubber particle size is, the more widely distributed it is in the sand column. It caused the weak interface, and the defects of the sand column are increased.

Second, bacteria are more likely to absorb sand particles than smooth rubber. Therefore, there is a weak surface that is not cemented between the sand particles and the rubber, and this weak surface is easier to form between the rubber and the rubber particles, as shown in Figure 9. Stress concentration effects would develop on these weak surfaces. When the structure of MRS was stressed,

the crack occurred first on the stress concentration effect point. Then, the crack continued to expand until the specimen failed. When rubber particles with smaller particle sizes are used, the stress concentration is more likely to occur through the weak interface of the rubber with small particle sizes. Therefore, under the same rubber content, the UCS of MRS decreased more obviously with a smaller rubber particle size.

Third, under the external load, the deformation of rubber particles produced tensile stress on the calcium carbonate and sand around the MRS. After MICP treatment, the tensile strength of the MRS was low, which caused tensile damage to the inside and the interface of the MRS, and accelerated the damage development of the internal structure. Under the same structural deformation conditions of MRS, rubber particles with small particle sizes could only withstand relatively small deformation, and the tensile failure of solidified samples was relatively obvious. The rubber particle has a tensile influence zone, and the size of the influence zone is proportional to the size of the rubber particle. Therefore, in the case of the same rubber content, although the tensile influence zone of smaller rubber particles is smaller, the number of rubber particles is larger (Figures 8B–D), which is more likely to cause multi-axial overlapping tensile damage in the same position. Therefore, $\omega$ of 0–1-mm MRS was higher than that of 1–2 mm and 2–3-mm MRS, but the UCS of 0–1 mm MRS was lower.

## 5 Conclusion

A series of water absorption and UCS tests were conducted to investigate the effect of different rubber particle sizes and contents on MRS. The following conclusions can be drawn from the study.

(1) For the 0–1-mm MRS, $\omega$ was the lowest when the rubber content was 5%. For the 1–2-mm and 2–3-mm MRS, $\omega$ decreased with the increase in the rubber content and reached the minimum when the rubber content was 9%. $\omega$ was reduced when the rubber content was larger, which inhibits the generation and development of initial cracks in the MICP-solidified samples.

(2) The UCS of 0–1-mm MRS decreased with the increase in the rubber content. When the rubber particle size was 1–2 mm and 2–3 mm, the UCS increased first and then decreased with the increase in the rubber content. The 1–2-mm and 2–3-mm MRS reached a peak value when the rubber content was 3% and 5%, respectively, which was increased by 11.3% and 15.69% compared to the clean sand, respectively.

(3) $\omega$ decreased with the increase in the $CaCO_3$ content with different particle sizes. It is indicated that MICP reinforcement can reduce open pores and internal cracks in the samples, which increased the cementation between sand particles. The degree of cementation increased with the increase in the $CaCO_3$ content. However, the UCS did not increase with the increase in the $CaCO_3$ content.

(4) Adding rubber can promote the formation of $CaCO_3$, resulting in a decrease in $\omega$ and increase in UCS. However, the rubber particles show lower strength and stiffness and are easy to aggregate, which caused the UCS to decrease at higher rubber content. A large amount of 0–1-mm rubber increased transverse deformation, which accelerated the destruction of the sand structure. $\omega$ of 0–1-mm MRS was higher than that of 1–2 mm and 2–3-mm MRS, but the UCS of 0–1-mm MRS was lower.

The effects of rubber content and particle size on the water absorption and UCS of MICP-solidified calcareous sand were discussed, and the mechanical mechanism of rubber combined MICP-solidified calcareous sand was analyzed. In conclusion, adding rubber in equal volume can reduce the pore defects of the sample, but this affects the UCS of the sample. The results of this study prove that the best rubber size is 1–2 mm and 2–3 mm, and the best rubber content is 3%–5%. It can provide a basis for the application of MICP-combined rubber reinforcement technology in island and reef engineering.

## Data availability statement

The original contributions presented in the study are included in the article/Supplementary Material; further inquiries can be directed to the corresponding author.

## Author contributions

XX: conceptualization, data curation, formal analysis, funding acquisition, project administration, resources, and writing–original draft. XY: investigation, methodology, project administration, software, supervision, validation, visualization, and writing–review and editing.

## Funding

The author(s) declare that financial support was received for the research, authorship, and/or publication of this article. This study was supported by the Dongguan Social Development Science and Technology Key Project (Project No. 20231800939992).

## Conflict of interest

The authors declare that the research was conducted in the absence of any commercial or financial relationships that could be construed as a potential conflict of interest.

## Publisher's note

# References


Aamir, M., Abdelmalek, B., and Gates, W. P. (2018). Improvement of coarse sand engineering properties by microbially induced calcite precipitation. *Geomicrobiol. J.* 35 (10), 887–897. doi:10.1080/01490451.2018.1488019

Anastasiadis, A., Senetakis, K., and Pitilakis, K. (2012). Small-strain shear modulus and damping ratio of sand-rubber and gravel-rubber mixtures. *Geotechnical Geol. Eng.* 30, 363–382. doi:10.1007/s10706-011-9473-2

ASTM (2017) *Standard practice for classification of soils for engineering purposes (unified soil classification system)*. West Conshohocken, PA: ASTM International. ASTM, D2487.

ASTM (2020) *Standard practice for use of Scrap tires in Civil engineering applications*. West Conshohocken, PA: ASTM International. ASTM, D6270.

Bai, B., Bai, F., Nie, Q., and Jia, X. (2023). A high-strength red mud–fly ash geopolymer and the implications of curing temperature. *Powder Technol.* 416 (15), 118242. doi:10.1016/j.powtec.2023.118242

Bai, B., Jiang, S., Liu, L., Li, X., and Wu, H. (2021). The transport of silica powders and lead ions under unsteady flow and variable injection concentrations. *Powder Technol.* 387, 22–30. doi:10.1016/j.powtec.2021.04.014

Castro-Alonso, M. J., Montañez-Hernandez, L. E., Sanchez-Muñoz, M. A., Macias Franco, M. R., Narayanasamy, R., and Balagurusamy, N. (2019). Microbially induced calcium carbonate precipitation (MICP) and its potential in bioconcrete: microbiological and molecular concepts. *Front. Mater.* 6, 126. doi:10.3389/fmats.2019.00126

Cheng, Y. J., Tang, C. S., Pan, X. H., Liu, B., Xie, Y. H., Cheng, Q., et al. (2021). Application of microbial induced carbonate precipitation for loess surface erosion control. *Eng. Geol.* 294, 106387. doi:10.1016/j.enggeo.2021.106387

Chu, J., Ivanov, V., Stabnikov, V., and Li, B. (2013). Microbial method for construction of an aquaculture pond in sand. *Geotechnique* 63 (10), 871–875. doi:10.1680/geot.sip13.p.007

Cui, M.-J., Zheng, J.-J., Dahal, B. K., Lai, H.-J., Huang, Z.-F., and Wu, C.-C. (2021). Effect of waste rubber particles on the shear behaviour of bio-cemented calcareous sand. *Acta Geotech.* 16, 1429–1439. doi:10.1007/s11440-021-01176-y

Cuthbert, M. O., McMillan, L. A., Handley-Sidhu, S., Riley, M. S., Tobler, D. J., and Phoenix, V. R. (2013). A field and modeling study of fractured rock permeability reduction using microbially induced calcite precipitation. *Environ. Sci. Technol.* 47 (23), 13637–13643. doi:10.1021/es402601g

DeJong, J. T., Fritzges, M. B., and Nusslein, K. (2006). Microbially induced cementation to control sand response to undrained shear. *J. Geotech. Geoenviron. Eng.* 132 (11), 1381–1392. doi:10.1061/(asce)1090-0241(2006)132:11(1381)

Fan, Y., Hu, X., Zhao, Y., Wu, M., Wang, S., Wang, P., et al. (2020). Urease producing microorganisms for coal dust suppression isolated from coal: characterization and comparative study. *Adv. Powder Technol.* 31 (9), 4095–4106. doi:10.1016/j.apt.2020.08.014

Frutos, I., García-Delgado, C., Gárate, A., and Eymar, E. (2016). Biosorption of heavy metals by organic carbon from spent mushroom substrates and their raw materials. *Int. J. Environ. Sci. Technol.* 13, 2713–2720. doi:10.1007/s13762-016-1100-6

Gersten, J., Fainberg, V., Garbar, A., Hetsroni, G., and Shindler, Y. (1999). Utilization of waste polymers through one-stage low-temperature pyrolysis with oil shale. *Fuel* 78 (8), 987–990. doi:10.1016/s0016-2361(99)00002-2

Harkes, M. P., van Paassen, L. A., Booster, J. L., Whiffin, V. S., and van Loosdrecht, M. C. M. (2010). Fixation and distribution of bacterial activity in sand to induce carbonate precipitation for ground reinforcement. *Ecol. Eng.* 36 (2), 112–117. doi:10.1016/j.ecoleng.2009.01.004

Hassanli, R., Youssf, O., Vincent, T., Mills, J. E., Manalo, A., and Gravina, R. (2020). Experimental study on compressive behavior of FRP-confined expansive rubberized concrete. *J. Compos. Constr.* 24 (4), 04020034. doi:10.1061/(asce)cc.1943-5614.0001038

Lee, S., Chung, M., Park, H. M., Song, K. I., and Chang, I. (2019). Xanthan gum biopolymer as soil-stabilization binder for road construction using local Soil in Sri Lanka. *J. Mater. Civ. Eng.* 31 (11), 06019012. doi:10.1061/(asce)mt.1943-5533.0002909

Li, P. (2021). Damping properties and microstructure analysis of microbial consolidated rubber sand. *Adv. Civ. Eng.* 2021, 1–7. doi:10.1155/2021/2338000

Liu, L., Liu, H. L., Xiao, Y., Chu, J., Xiao, P., and Wang, Y. (2017). Biocementation of calcareous sand using soluble calcium derived from calcareous sand. *Bull. Eng. Geol. Environ.* 77 (4), 1781–1791. doi:10.1007/s10064-017-1106-4

Ma, G. L., He, X., Jiang, X., Liu, H. L., Chu, J., and Xiao, Y. (2021). Strength and permeability of bentonite-assisted biocemented coarse sand. *Can. Geotech. J.* 58 (7), 969–981. doi:10.1139/cgj-2020-0045

Montoya, B. M., and DeJong, J. T. (2015). Stress-strain behavior of sands cemented by microbially induced calcite precipitation. *J. Geotech. Geoenviron. Eng.* 141 (6), 10. doi:10.1061/(asce)gt.1943-5606.0001302

Montoya, B. M., Dejong, J. T., and Boulanger, R. W. (2013). Dynamic response of liquefiable sand improved by microbial-induced calcite precipitation. *Geotechnique* 63 (4), 302–312. doi:10.1680/geot.sip13.p.019

Nosouhian, F., Mostofinejad, D., and Hasheminejad, H. (2016). Concrete durability improvement in a sulfate environment using bacteria. *J. Mater. Civ. Eng.* 28 (1), 04015064. doi:10.1061/(asce)mt.1943-5533.0001337

O'Donnell, S. T., and Kavazanjian, E. (2015). Stiffness and dilatancy improvements in uncemented sands treated through MICP. *J. Geotech. Geoenviron. Eng.* 141 (11), 02815004. doi:10.1061/(asce)gt.1943-5606.0001407

Omoregie, A. I., Ouahbi, T., Ong, D. E. L., Basri, H. F., Wong, L. S., and Bamgbade, J. A. (2024). Perspective of hydrodynamics in microbial-induced carbonate precipitation: a bibliometric analysis and review of research evolution. *Hydrology* 11 (5), 61. doi:10.3390/hydrology11050061

Omoregie, A. L., Ong, D. E. L., Li, P. Y., Senian, N., Hei, N. L., Esnault-Filet, A., et al. (2023). Effects of push–pull injection–suction spacing on sand biocementation treatment. *Geotechnical Res.* 11 (1), 28–42. doi:10.1680/jgere.22.00053

Phillips, A. J., Cunningham, A. B., Gerlach, R., Hiebert, R., Hwang, C. C., Lomans, B. P., et al. (2016). Fracture sealing with microbially-induced calcium carbonate precipitation: a field study. *Environ. Sci. Technol.* 50 (7), 4111–4117. doi:10.1021/acs.est.5b05559

Riveros, G. A., and Sadrekarimi, A. (2020). Liquefaction resistance of Fraser River sand improved by a microbially-induced cementation. *Soil Dyn. Earthq. Eng.* 131, 106034. doi:10.1016/j.soildyn.2020.106034

Saleem, M., Shameem, M., Hussain, S., and Maslehuddin, M. (1996). Effect of moisture, chloride and sulphate contamination on the electrical resistivity of Portland cement concrete. *Constr. Build. Mater.* 10 (3), 209–214. doi:10.1016/0950-0618(95)00078-x

Shahnazari, H., and Rezvani, R. (2013). Effective parameters for the particle breakage of calcareous sands: an experimental study. *Eng. Geol.* 159, 98–105. doi:10.1016/j.enggeo.2013.03.005

Shan, Y., Liang, J. L., Tong, H. W., Yuan, J., and Zhao, J. T. (2022a). Effect of different fibers on small-strain dynamic properties of microbially induced calcite precipitation-fiber combined reinforced calcareous sand. *Constr. Build. Mater.* 322, 126343. doi:10.1016/j.conbuildmat.2022.126343

Shan, Y., Zhao, J., Tong, H., Yuan, J., Lei, D., and Li, Y. (2022b). Effects of activated carbon on liquefaction resistance of calcareous sand treated with microbially induced calcium carbonate precipitation. *Soil Dyn. Earthq. Eng.* 161, 107419. doi:10.1016/j.soildyn.2022.107419

Stocks-Fischer, S., Galinat, J. K., and Bang, S. S. (1999). Microbiological precipitation of $CaCO_3$. *Soil Biol. Biochem.* 31 (11), 1563–1571. doi:10.1016/s0038-0717(99)00082-6

Su, H., Xiao, H., Li, Z., Tian, X., Luo, S., Yu, X., et al. (2022). Experimental study on microstructure evolution and fractal features of expansive Soil improved by MICP method. *Front. Mater.* 9, 842887. doi:10.3389/fmats.2022.842887

van Paassen, L. A., Ghose, R., van der Linden, T. J. M., van der Star, W. R. L., and van Loosdrecht, M. C. M. (2010). Quantifying biomediated ground improvement by ureolysis: large-scale biogrout experiment. *J. Geotech. Geoenviron. Eng.* 136 (12), 1721–1728. doi:10.1061/(asce)gt.1943-5606.0000382

Wang, S., Lei, X.-W., Meng, Q.-S., Xu, J.-L., Xie, L.-F., and Li, Y.-J. (2020). Influence of particle shape on the density and compressive performance of calcareous sand. *KSCE J. Civ. Eng.* 24 (1), 49–62. doi:10.1007/s12205-020-0145-8

Wang, X. Z., Jiao, Y. Y., Wang, R., Hu, M. J., Meng, Q. S., and Tan, F. Y. (2011). Engineering characteristics of the calcareous sand in nansha islands, South China sea. *Eng. Geol.* 120 (1-4), 40–47. doi:10.1016/j.enggeo.2011.03.011

Wang, Z., Zhang, N., Cai, G., Jin, Y., Ding, N., and Shen, D. (2017). Review of ground improvement using microbial induced carbonate precipitation (MICP). *Mar. Georesources Geotechnol.* 35 (8), 1135–1146. doi:10.1080/1064119x.2017.1297877

Whiffin, V. S., van Paassen, L. A., and Harkes, M. P. (2007). Microbial carbonate precipitation as a Soil improvement technique. *Geomicrobiol. J.* 24 (5), 417–423. doi:10.1080/01490450701436505

Xiao, P., Liu, H. L., Xiao, Y., Stuedlein, A. W., and Evans, T. M. (2018). Liquefaction resistance of bio-cemented calcareous sand. *Soil Dyn. Earthq. Eng.* 107, 9–19. doi:10.1016/j.soildyn.2018.01.008

Xiao, Y., He, X., Evans, T. M., Stuedlein, A. W., and Liu, H. L. (2019). Unconfined compressive and splitting tensile strength of basalt fiber-reinforced biocemented sand. *J. Geotech. Geoenviron. Eng.* 145 (9), 04019048. doi:10.1061/(asce)gt.1943-5606.0002108

Xiao, Y., Xiao, W. T., Ma, G. L., He, X., Wu, H. R., and Shi, J. Q. (2022). Mechanical performance of biotreated sandy road bases. *J. Perform. Constr. Facil.* 36 (1), 04021111. doi:10.1061/(asce)cf.1943-5509.0001671

Yuan, J., Lei, D. L., Shan, Y., Tong, H. W., Fang, X. T., and Zhao, J. T. (2022). Direct shear creep characteristics of sand treated with microbial-induced calcite precipitation. *Int. J. Civ. Eng.* 20, 763–777. doi:10.1007/s40999-021-00696-8

Zhao, J. T., Shan, Y., Tong, H. W., Yuan, J., and Liu, J. M. (2022). Study on calcareous sand treated by MICP in different NaCl concentrations. *Eur. J. Environ. Civ. Eng.* 1-20. doi:10.1080/19648189.2022.2130439

Zhao, J. T., Tong, H. W., Shan, Y., Yuan, J., Peng, Q. W., and Liang, J. L. (2021). Effects of different types of fibers on the physical and mechanical properties of MICP-treated calcareous sand. *Materials* 14 (2), 268. doi:10.3390/ma14020268

Zhao, Y., Fan, C., Liu, P., Fang, H., and Huang, Z. (2018). Effect of activated carbon on microbial-induced calcium carbonate precipitation of sand. *Environ. Earth Sci.* 77, 615. doi:10.1007/s12665-018-7797-4

Zhao, Y., Xiao, Z. Y., Fan, C. B., Shen, W. Q., Wang, Q., and Liu, P. H. (2020). Comparative mechanical behaviors of four fiber-reinforced sand cemented by microbially induced carbonate precipitation. *Bull. Eng. Geol. Environ.* 79 (6), 3075–3086. doi:10.1007/s10064-020-01756-4

Zhou, Z., Lin, H., and Liu, J. (2023). "Experimental and numerical investigations on the compression behavior of calcareous sand-rubber mixture," in *Proceedings of the 2022 international conference on green building, Civil engineering and smart city*. Editors W. Guo, and K. Qian (Springer), 211.